WILEY-VCH

Mixed Anionic and Cationic Redox Chemistry in a Tetrathiomolybdate Amorphous Coordination Framework

*Qi Zhu, Jiande Wang, Xuelian Liu, Dr. Neil Ebejer, Dr. Darsi Rambabu, and Prof. Alexandru Vlad**

Institute of Condensed Matter and Nanosciences, Molecular Chemistry, Materials and Catalysis, Université catholique de Louvain, Louvain-la-Neuve B-1348, Belgium

E-mail: alexandru.vlad@uclouvain.be

Abstract

We report the electrochemistry of a hitherto unexplored Na_2MoS_4 phase as conversion electrode material for Na- and Li-cation reversible storage. The material adopts an amorphous coordination polymer structure, with mixed Mo and S valences. Ex-situ XPS and in-situ XRD analysis reveal a complex interplay between Mo and S redox, while excluding the formation of free sulfur, lithium sulfide or other crystalline phases. Na_2MoS_4 behaves as a mixed ionic-electronic conductor, with electronic conductivity of 6.1 × 10^{-4} S cm^{-1}, that allowed the use of this material without any conductive carbon in an electrochemical cell. A reversible capacity of 500 mAh g^{-1} is attained corresponding to 5-electron redox exchange, with the end-member reaching from $Na_{<1}MoS_4$ to $Na_{>5}MoS_4$. This study not only emphasizes on the excellent charge storage performances of Na_2MoS_4 for Li or Na batteries, but also enriches the emerging library and knowledge of sulfide phases with mixed anionic and cationic redox.

Angewandte Chemie International Edition
10.1002/anie.202004587

Introduction

The ever-increasing demand for energy storage devices with high energy and power density is currently driven by the fast development of electric vehicles and portable electronic devices. As a typical example of energy storage, Li-Ion Batteries (LIBs) exhibit great potential and attract more and more attention given their high energy density, relatively low cost and limited environmental impact.[1] Despite the major achievements in the development of LIBs in recent decades, the advancement of battery technology remains nevertheless incremental.[2–6] In commercial LIBs, graphite and lithium metal oxides are commonly employed as negative and positive electrode materials, respectively. Amongst the most used positive electrode chemistries, the layered rock salt structure $LiCoO_2$ (LCO) can deliver a reversible capacity of 140 mAh g^{-1} while higher capacities lead to structure collapse,[7,8] unless surface coating strategies are utilized.[9] Ternary cathode material $LiNi_xMn_yCo_zO_2$ (NMC) class has been found to alleviate the issues of LCO and is now extensively applied as positive electrode material in most commercial LIBs.[10]

The need for higher energy density however continuously challenged these materials, culminating with the extension of the redox beyond solely that of the transition metal.[11,12] Anionic redox chemistry has thus emerged as a means to considerably increase the energy density, whereby the capacity is a combined contribution from the oxidation of O^{2-} to peroxo-like species O_2^{2-} along with transition metal redox. Although electrochemical participation of the oxygen has brought higher energy densities, intrinsic issues such as poor kinetics, voltage fade, and irreversible oxygen loss cannot be ignored. Some effective methods have been applied to overcome this, for example with $Li_2Ru_{1-y}Sn_yO_3$[12] stabilizing the O redox by introducing a 4d instead of 3d transition metal and increasing the Li participation to access higher capacities, which are electrochemically similar to Li-rich NMC[13,14] but have simpler redox chemistry.

To conquer the intrinsic issues of oxygen anionic redox, replacement by the less electronegative sulfur was recently proposed and is gaining importance since sulfur has been found to effectively inhibit anion loss whilst also showing higher reversibility with lower hysteresis during cycling.[15-17] Shadike *et al.* have studied the electrochemistry of $NaCrS_2$ relying only on sulfur anionic redox by blocking the transition metal redox. This material was found to provide a capacity of 95 mAh g^{-1} and although it cannot solve the issue of low capacities, it remains a model sulfide redox chemistry.[15] Therefore, the cation redox in the sulfide compounds was also targeted in pursuit of perfect sulfide anion redox chemistries. Wang *et al.* reported on O3-$NaCr_{2/3}Ti_{1/3}S_2$ that was found to deliver higher reversible

capacities of 186 mAh g^{-1} (0.95 Na) based on cumulative, cation and anion redox process.[16] Recently, Tarascon *et al.* presented a fundamental research on the bottlenecks of sulfur redox,[17] in which a new material $Li_{1.33-2y/3}Ti_{0.67-y/3}Fe_yS_2$ (y = 0.3) was shown to deliver a reversible capacity as high as 245 mAh g^{-1}. The high capacity resulted from the existence of $3d^6$ electrons in $Fe^{2+/3+}$ redox couple that activated the anionic sulfur redox. During the final review stage of this manuscript, See *et al.*, revealed the electrochemistry of a lithium-rich layered iron sulfide Li_2FeS_2,[18],whereas Zhao-Karger reported on multivalent cation storage in VS_4,[19] further emphasizing the rising importance of this class of materials.

It should be noted however, that transition metal sulfides with mixed cation and anion redox are not new, and were first pioneered by Rouxel in late 90's,[20] with many sulfide chemistries such as TiS_3, FeS_2, VS_4, and $LiMS_2$ (M=Ti, V, Cr, Fe) known for decades[21–24]. In these, sulfur can fully or partially exist in the S_2^{2-} state (via S^-–S^- bonds) and thus can undergo a reversible electrochemical transformation ($S_2^{2-} \rightarrow 2S^{2-}$). However, irreversible anion redox reactions also lead to capacity fade in these chemistries. Molybdenum-sulfide chemistry has also been extensively explored for electrochemical charge storage, with particularly increased focus since the discovery of 2D phases and morphologies (e.g. MoS_2).[25] Tetrathiomolybdate (MoS_4^{2-}) chemistry however received little attention for electrochemical energy storage, despite a broad range of compositions being reported for this parent anion chemistry.

A highly oxidized phase of the MoS_4^{2-}, presented as MoS_4, was reported by Khudorozhko *et al.*[26] This was obtained by thermal dissociation of $(NH_4)_2Mo_2S_{12}•2H_2O$. Ten years earlier, Abraham studied a similar composition, yet based on a Selenium doped $MoSe_3S$ phase.[27,28] The respective studies focused on Li^+ intercalation and electronic structure investigations, starting with the parent MoS_4 phases. Considering these, it could be presumed that MoS_4^{2-} can undergo a two-electron oxidation process, through predominantly S^{2-} redox, and form a stable MoS_4 phase. However, according to Belanger *et al.*[29] and Bhattacharya *et al.*[30], who studied the composition of films prepared by anodic electrodeposition from both, non-aqueous and aqueous solutions of $(NH_4)_2MoS_4$, MoS_4 is not a pure phase, but is composed of amorphous MoS_3 and elemental sulfur (S_8). This clearly indicates that the full, two-electron oxidation of MoS_4^{2-} is a non-reversible process. Lower valences for Mo and S in MoS_4^{2-} have also been disclosed in the same work by Khudorozhko[26] reporting on rich lithiated phases of up to Li_7MoS_4 in composition, prepared however, by chemical lithiation.

It is in fact based on Khudorozhko's work that we started our investigation of these particular materials, interested by their potentially rich electrochemistry. Considering that by chemical lithiation the authors proposed a stepwise conversion from a MoS_4 phase into a lithium-rich Li_7MoS_4 phase, we envisioned that an electrode material with potentially 7 electrons and 7 Li cations, corresponding to an impressive storage capacity of almost 700 mAh g^{-1}, could be obtained. Additionally, mixed S anionic and Mo cationic redox would have been a plausible route for the massive 7-electron exchange per formula unit. However, the work of Belanger and Bhattacharya made us abandon the search of the fully oxidized "MoS_4 phase" and we started searching for possible MoS_4^{x-} species with alkali metal cation content.

Sodium tetrathiomolybdate (Na_2MoS_4) was identified as a potentially interesting candidate. This chemistry was reported by Laurie *et al.* in 1984, while studying the toxicity of the tetrathiomolybdate with different cations.[31] However, to the best of our knowledge, no studies were carried out on the applicability of this material for energy storage. Herein, we report on the electrochemistry of a sodium tetrathiomolybdate phase with a nominal composition of Na_2MoS_4 (hereafter noted as <Na_2MoS_4>, since the single phase composition is still not confirmed) as a promising electrode material for room temperature rechargeable SIBs and LIBs. The material adopts an amorphous coordination polymer framework with mixed valence as determined by XPS. Due to combined cation ($Mo^{6+} \rightarrow Mo^{2+}$) and anion ($S^{2-} \rightarrow S_2^{2-}$) redox, this material can exchange up to 5 electrons, corresponding to a theoretical capacity of 495 mAh g^{-1}. Full alkali ion extraction is not possible, and only one equivalent was possible to reversibly extract and cycle, largely based on sulfide anionic redox. Interestingly, the pristine <Na_2MoS_4> composition is also electrically conducting, enabling us to build and cycle cells without any conductive additive. In both, Li and Na cells, the <Na_2MoS_4> based electrodes show a high capacity retention of more than 270 mAh g^{-1} with high coulombic efficiency in average of 99.9% after 200 cycles.

Results and Discussion

The method for Na_2MoS_4 synthesis in this work was adopted from previous reports and consisted of two steps (refer to SI, Experimental Section): (i) the synthesis of the ammonium tetrathiomolybdate $(NH_4)_2MoS_4$ precursor;[32] followed by (ii) the synthesis of sodium tetrathiomolybdate hydrate salt ($Na_2MoS_4 \cdot 3.5H_2O$), as expressed by Equations 1 and 2, respectively. The crystal structure of synthesized $Na_2MoS_4 \cdot 3.5H_2O$ was confirmed by PXRD, and was found to match the JCPDS card No. 00-038-0076 (Fig. S1), indicating the successful preparation of the $Na_2MoS_4 \cdot 3.5H_2O$ crystalline phase. The hydrated phase is soluble in

aprotic electrolytes and side-reactions are observed (hydrolysis of $LiPF_6$ and subsequent side reactions,[33,34] Figure S2) so that an additional dehydration step was required (Eq. 3). The dehydration step was found however to alter significantly the crystal structure of the material and is discussed next.

$$(NH_4)_6Mo_7O_{24}{\cdot}4\ H_2O + 28\ (NH_4)_2S \rightarrow 7\ (NH_4)_2MoS_4 + 48\ NH_3 + 28\ H_2O \quad \text{(Eq.1)}$$

$$(NH_4)_2MoS_4 + 2NaOH\ (aq) \rightarrow Na_2MoS_4{\bullet}3.5H_2O + 2NH_3 \quad \text{(Eq.2)}$$

$$Na_2MoS_4{\bullet}3.5H_2O \rightarrow <Na_2MoS_4> + H_2O \quad \text{(Eq.3)}$$

Scheme 1. Synthesis steps of amorphous <Na_2MoS_4> phase.

Thermogravimetric analysis (TGA) was applied to monitor the evolution of dehydration process, along with PXRD analysis of samples annealed at different temperatures (Figs. 1A, 1B). A weight loss of around 20% is occurring from 55 to 120 °C associated with two endothermic signals from DSC, corresponding to the removal of the 3.5 equivalents of H_2O. The loss of crystalline water was accompanied by structure collapse and gradual conversion to an amorphous phase. The color also changed from red to black during the dehydration process (Fig. S2). The obtained <Na_2MoS_4> phase is amorphous, with the formula composition semi-quantitatively confirmed by EDX analysis (Fig. S3). The FTIR spectra also confirms the removal of water from $Na_2MoS_4{\bullet}3.5H_2O$, with the disappearance of the characteristic water bands at 3450 and 1580 cm^{-1} (Fig. 1C). This process also alters the valences of Mo and S, as determined from XPS analysis (refer further to Fig. 3 and Table 1). Solubility in aprotic polar solvent (carbonate or ether based electrolytes) was also found to be significantly affected, with the pristine $Na_2MoS_4{\bullet}3.5H_2O$ being highly soluble, whereas the dehydrated phase showing no signs of solubility (Fig. S2).

The formation of an amorphous coordination polymer phase is the most plausible explanation at this stage to the experimental data, similar to recently studied *a*-(Mo_3S_{11}) phases by Truong *et al*[35] and Hung *et al.*[36] Further studies and use of advanced techniques are required to get a better understanding of the structure of the <Na_2MoS_4> phase, or possible co-existence of several phases, but it can be assumed at this stage that the MoS_4 units are connected via ionic or coordination bonds, as well covalent disulfide bonds (as confirmed by XPS and the appearance of the S–S vibration band in FTIR, Fig. 1C). Compared to pristine

Na_2MoS_4•3.5H_2O, the <Na_2MoS_4> phase is also not stable in ambient air, and undergoes an oxidative hydrolysis resulting in the formation of Na_2MoO_4 (Fig. S4).

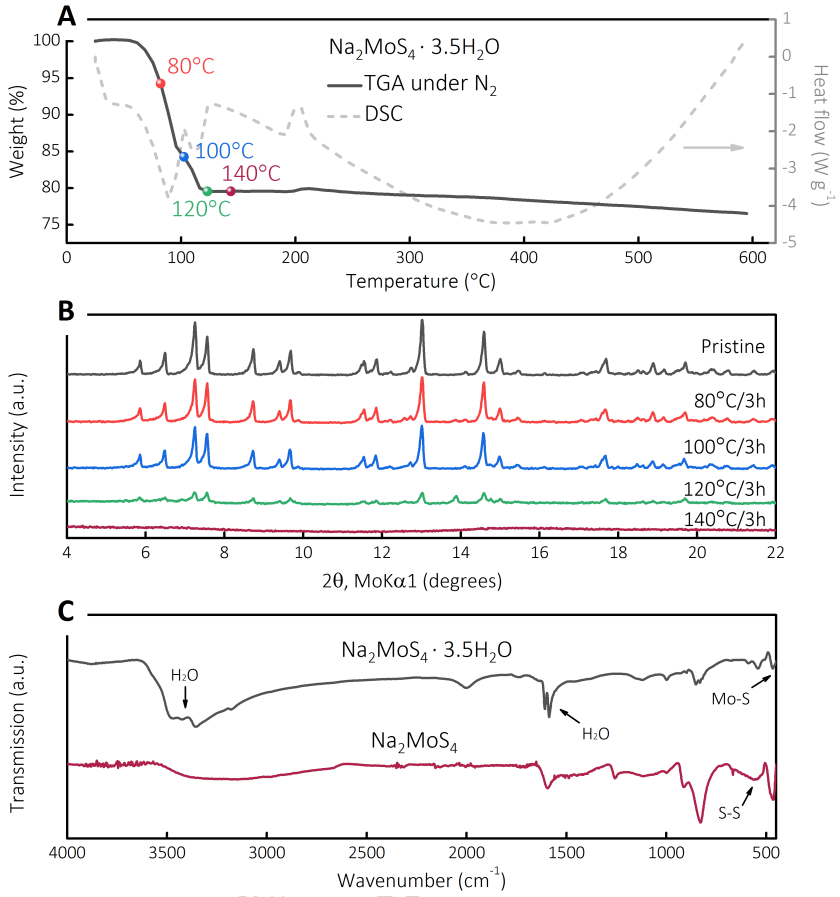

Figure 1. Synthesis and physico-chemical characterization of the <Na_2MoS_4> phase. (A) Overlaid TGA and DSC plots and, (B) the PXRD temperature-dependent survey of the dehydration process. (C) FTIR plots of Na_2MoS_4•3.5H2O and dehydrated <Na_2MoS_4>.

The electrochemistry of <Na_2MoS_4> was assessed in both, Na and Li half-cell configuration and typical potential - composition profiles, as well as cycling stability for galvanostatic cycling tests are shown in Figure 2. All cells displayed an OCP (open circuit potential) in the 1.8 – 2.2 V vs. Li^+/Li^0 or Na^+/Na^0 (marked with a dot in Figs. 2A, 2B), consistent with the reactivity towards oxygen and moisture, as well as with the presence of S_2^{2-} species (Figs. 1C, 3C). The first discharge process (marked with an arrow in Figs. 2A and 2B) delivers a capacity of about 330 and 290 mAh g^{-1} for Li and Na storage, respectively. Upon charging, similar capacities are obtained up to a charge potential equivalent to the initial OCP, with extra capacity attained by extending the cycling window to 3V (vs. Li^+/Li^0) or 2.7V (vs. Na^+/Na^0). The cycling stability is excellent, and a capacity of more than 400 mAh g^{-1} is retained after 50 cycles at a slow cycling rate of C/10 (for 1 electron transfer capacity in

one hour, 1C rate corresponds to 99 mA/$g_{of\ Na2MoS4}$) for the Li cell (Fig. 2C). Similar capacities are also achieved for Na cells, with slightly faster degradation after first 10 cycles (at a rate of C/10), probably resulting from the interferences with electrolyte degradation species generated at the metallic Na counter-electrode.

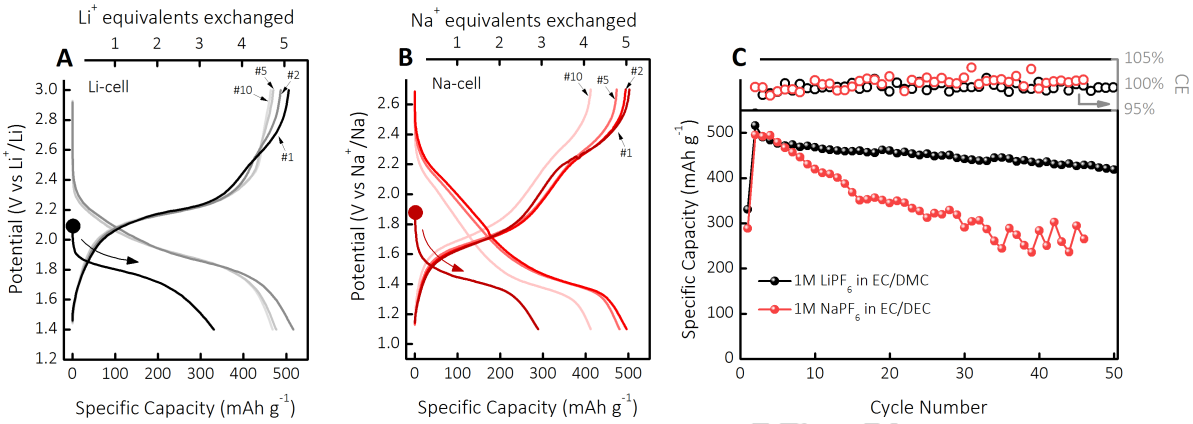

Figure 2. Electrochemistry of <Na_2MoS_4>. Charge/discharge profiles at a cycling rate of C/10 (equivalent of 5 electrons transferred in 10 h) in Li (A) and Na (B) half-cell configurations. The potential window was adjusted for both so that the equivalent redox states are accessed: 1.4 - 3.0 V vs. Li^+/Li^0 (A) and 1.1 - 2.7 V vs. Na^+/Na^0 (B). The initial OCP and cycling direction are mentioned by the respective dots and arrows. (C) Capacity retention with cycling for the respective cells.

It should be noted that initial cycles for both Li and Na cell chemistries, display similar efficiencies, polarization and attainable capacities, implying that both, Li^+ or Na^+ - cation ingress/removal within the tetrathiomolybdate framework proceed efficiently and that the cation nature seems to have reduced impact on the conversion process, consistent with the amorphous nature of this material. Some differences can be however observed with a better-defined plateau around 2.3 V (*vs.* Na^+/Na^0), whereas for Li-cells the same gradually disappears. Additional consistent insight is provided by CV and *dQ*/*dV* plots (Fig. S5). A two pair of redox peaks is visible for both, Na- and Li- cells during the initial cycle. Whereas this is maintained for Na-cells, the higher voltage peak becomes weaker in the second cycle for Li-cells. The alkali cation ionic potential should alter the charge distribution and density of the tetrathiomolybdate framework and consequently the redox response. In the case of Li-cells, the cation mixing and progressive exchange (Na^+ by Li^+) leads indeed to changes in the galvanostatic profile during the first cycles with a subsequent stable profile attained. Since Li cells displayed much better stability and consistency (Figs. 2, S6), we focused primarily on this type of cell whilst currently working on understanding the degradation and improving the stability in Na cells.

The <Na_2MoS_4> - Li half-cells were subsequently operated in the specific potential windows (with respect to the OCP of the assembled cells), with supposed predominant anionic redox of $S^{2-} \leftrightarrow S_2^{2-}$ (Fig. 3A) and cationic redox of $Mo^{y+} \leftrightarrow Mo^{x+}$ (Fig. 3B). When operated in the 2–3 V (*vs*. Li^+/Li^0) window, stable and reversible cycling was obtained, corresponding to 1.2 equivalents of Na^+ extraction at the first cycle. The second Na cation could be also extracted, at a higher potential of 3.6 V (*vs*. Li^+/Li^0). However, this resulted in degradation, rapid loss of capacity and with the discharge profile not tracing back the charge profile (Fig. S7). Despite being made in different conditions (alkali cations, carbonate electrolyte, solid-phase electrochemical reaction) this result is consistent with work by Belanger[29] and Bhattacharya[30], in that the electrochemical oxidation of $(NH_4)_2MoS_4$ in both, aqueous and non-aqueous solution produced a material with $MoS_{3.8}$ stoichiometry, that however consisted of amorphous MoS_3 and elemental S_8. A stable and reversible capacity of around 110 mAh g^{-1} is attained in the limited electrode potential range of 2 – 3 V vs Li^+/Li^0, with more than 300 mAh g^{-1} attained in the cathodic scan range of 1.4 – 2.25 V vs Li^+/Li^0 (Figs. 3A, 3B). The summed capacity is consistent with the value in the full potential window as shown in Figure 2. It is also interesting to note the much better cycling stability in the 2 – 3 V window (albeit with lower Coulombic efficiency) as compared to lower electrode potential cycling window (Fig. S8), the origins of which are not well understood at this stage.

To decipher what processes are at play as a function of electrode potential, XPS was used to characterize the Mo and S valences of the as-synthesized materials as well as during cycling. Based on simple valence estimation, the redox state of Mo and S in the pristine $Na_2MoS_4 \cdot 3.5H_2O$ or <Na_2MoS_4> phases should be of +6 and -2, respectively. Accordingly, any anodic (oxidation) process of <Na_2MoS_4> could be expected to proceed predominantly through anionic sulfur redox, whereas cathodic (reduction) predominantly through redox on Mo. However, the oxidation when exposed to air and the appearance of a minor S–S band in FTIR (Fig. 1C) prompted for further in depth analyses of Mo and S valences by XPS. All binding energies were calibrated to the carbon 1s peak at 284.8 eV. The pristine $Na_2MoS_4 \cdot 3.5H_2O$ and <Na_2MoS_4> phases are discussed first (Fig. 3C configuration "*p*", and Fig. S9). The Mo 3d and S 2p XPS spectra are composed of Mo $3d_{5/2}$ - Mo $3d_{3/2}$ and S $2p_{3/2}$ - S $2p_{1/2}$ doublets. The integral intensities of their components correspond to 3:2 (Mo, $3d_{5/2}$: $3d_{3/2}$) and 2:1 (S, $2p_{3/2}$: $2p_{1/2}$). The spin-orbit splitting (the difference between Mo $3d_{5/2}$ and Mo $3d_{3/2}$ binding energies) is 3 eV, and 1 eV between S $2p_{3/2}$ and S $2p_{1/2}$.[37,38] The analysis shows that already in the hydrated crystalline phase of $Na_2MoS_4 \cdot 3.5H_2O$, the valences of Mo and S are different from as expected, with average estimated Mo oxidation state of +5.1,

whereas S being at -1.8. Upon dehydration, the valence state of Mo is further reduced to 4.7 whereas of S increases to -1.7, indicating a non-negligible disulfide bonding.

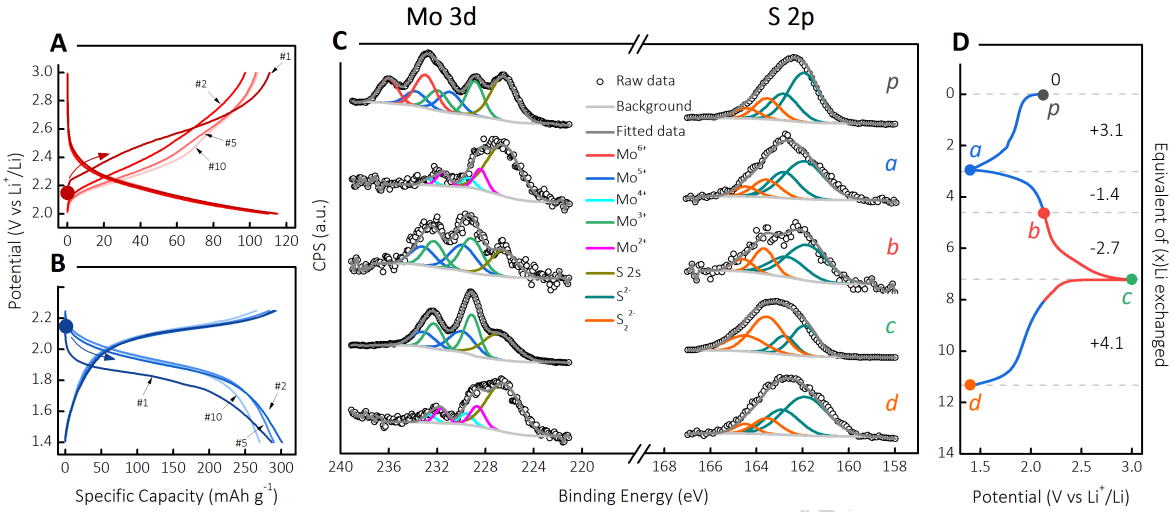

Figure 3. Ex-situ XPS Mo 3d and S 2p survey of mixed anionic and cationic redox in Na_2MoS_4. (A,B) Potential - capacity profiles for predominantly anionic and cationic redox processes in pristine <Na_2MoS_4> as electrode material in Li half-cell. (C) XPS spectra of Mo 3d and S 2p region for different state-of-charge with (D) the corresponding typical voltage - composition profile for the ex-situ XPS experiment.

To further probe the valence changes and illustrate the anionic and cationic redox mechanism in <Na_2MoS_4>, ex-situ electrochemical XPS analysis was performed and the results are shown in Figure 3, with the estimated valence states analysis resumed in Table 1. As a general observation, the position of the Mo 3d and S 2p peaks significantly shift during the redox process, suggesting changes in the Mo and S valence states. The four peaks in the initial Mo 3d spectrum (Fig. 3C, ***p*** corresponding to pristine <Na_2MoS_4>) are quantitatively deconvoluted to three doublets corresponding to Mo^{6+} (236 eV, Mo $3d_{3/2}$ and 233 eV, Mo $3d_{5/2}$), Mo^{5+} (233.8 eV, Mo $3d_{3/2}$ and 230.9 eV, Mo $3d_{5/2}$), Mo^{3+} (231.9 eV, Mo $3d_{3/2}$ and 228.8 eV, Mo $3d_{5/2}$), respectively. The estimated average valence of Mo is +4.7 in this case. The S 2p spectrum shows two doublets, corresponding to S^{2-} (162.5 eV, S $2p_{1/2}$ and 161.9 eV, S $2p_{3/2}$) and S_2^{2-} (164.3 eV, S $2p_{1/2}$ and 163.4 eV, S $2p_{3/2}$)[39] with an average S valence of -1.7. At the first reduction step, from ***p*** (2.1V) to ***a*** (1.4 V), the two dominant peaks of Mo^{6+} and Mo^{5+} disappear, while Mo^{4+} and Mo^{2+} emerge, additionally accompanied by changes in S 2p spectra. The 3.1 injected electrons result in a simultaneous reduction of Mo ($Mo^{4.7+}$ to $Mo^{2.6+}$) with nearly complete reduction of S to sulfide species ($S^{1.7-}$ to $S^{1.9-}$). On oxidation (***a*** → ***b*** → ***c***) the two peaks of Mo^{5+} and Mo^{3+} appear in the Mo 3d spectrum whilst vanishing for Mo^{4+} and Mo^{2+}, whereas the new peak with the binding energy at around 164 eV splits and appears associated with the of S_2^{2-} signal increase. The averaged estimated valence change during the

oxidation is more pronounced for Mo ($Mo^{2.6+}$ to $Mo^{3.9+}$) than for $S^{1.9-}$ (no valence change) during the initial re-charge process (1.4V to 2.1V, ***a*** → ***b***). Further from ***b*** to ***c*** (2.1 V to 3 V), minor changes are seen in the peak position and valence in Mo 3d spectrum. In contrast, a significant shift in the peak position for S 2p to higher binding energy is observed, associated with of S_2^{2-} increase and thus to sulfide oxidation ($S^{1.9-}$ to $S^{1.2-}$). In the following discharge step (back to 1.4 V, ***c*** → ***d***), the XPS pattern and peak deconvolution of Mo 3d and S 2p spectra return to the same position as for state ***b***, proving the full reversibility of the redox process.

phase	***x*** in (Mo^{x+})	***y*** in (S^{y-})	***z*** in (MoS_4^{z-})
hydrated	5.1	1.8	2
p	4.7	1.7	2
a	2.6	1.9	5.1
b	3.9	1.9	3.7
c	3.9	1.2	1
d	2.6	1.9	5.1

Table 1. XPS estimated Mo and S valence states during conversion process.

It should be mentioned that given the better stability of <Na_2MoS_4> in Li half-cells, XPS analysis was performed in this configuration, and that Na/Li cation exchange is inevitable during the reduction and oxidation processes. Although accurate determination of Li and Na content was not possible, it is reasonable to assume that the Li-to-Na ratio for compositions corresponding to configurations in ***a*** and ***d*** is considerably increased (Li^+ uptake ***p*** → ***a***, followed by mixed Li^+/Na^+ removal ***a*** → ***b*** → ***c***, followed again by Li^+ uptake ***c*** → ***d***). No significant differences can be observed in the XPS data and analysis of compositions in ***a*** and ***d*** (Figure 3C) so that we can reasonably assume that the nature of the alkali cation has a limited impact on the XPS data and analysis with similar results (S and Mo valences) possibly attained for solely Na-cation ingress/removal.

Additional insight into the electrochemistry of <Na_2MoS_4> while excluding any potential irreversible side-reaction and formation of additional redox active phases (like elemental sulfur - S_8, lithium disulfide - Li_2S) was provided by in-situ electrochemical XRD (Fig. 4A). Besides two sharp peaks originating from Li counter-electrode and stainless steel from the

cell construct and measurement set-up (in-house fabricated coin-cells for XRD transmission configuration, refer to SI ,Fig. S10), only a broad signal is observed, resulting from the amorphous phases in the composite electrode including conductive carbon and <Na_2MoS_4>. The PXRD patterns of possible generated phases (e.g. Li_2S, Na_2S, and S_8) are displayed in panel 4B. Perceptibly, no similar peaks appear during the electrochemical cycling, confirming that <Na_2MoS_4> does not decompose into any of these whilst the amorphous phase of <Na_2MoS_4> is maintained during the alkali metal ion ingress or extraction. It is also noted, that the intensity of the Li (110) peak (marked with *) evolves according to the charge/discharge process, reflecting the plating and stripping of Li metal at the counter electrode.

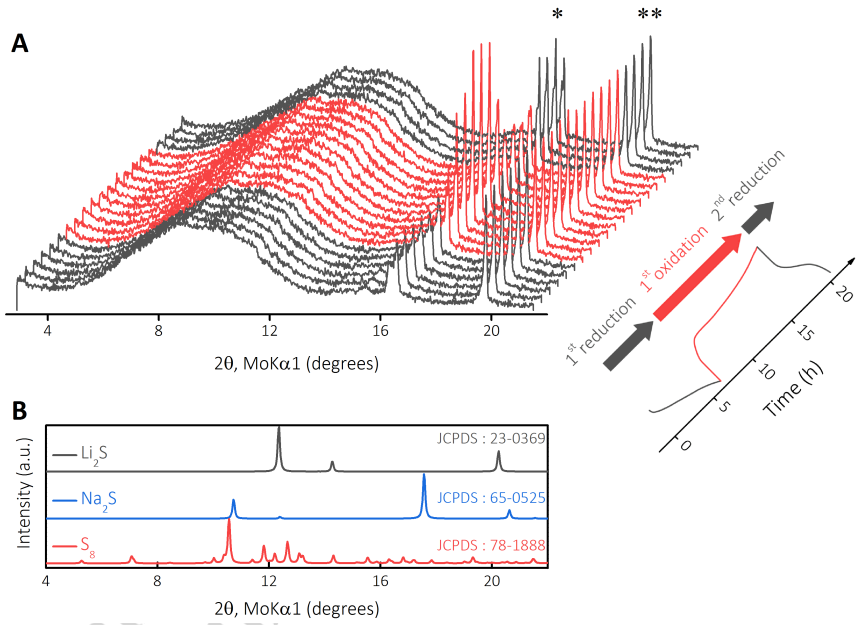

*Figure 4. In-situ electrochemistry - XRD survey. (A) XRD pattern evolution with cycling (plot to the right) measured in transmission mode. The peaks marked with * and ** correspond to Li (110) and stain steel diffraction peaks from the in-situ cell construct, respectively. (B) PXRD patterns for Li_2S, Na_2S and S_8 phases aligned to in-situ data, confirming the absence of the respective phases during electrochemical conversion reaction.*

The mixed cation and anion valences in $Na_2MoS_4 \cdot 3.5H_2O$ and <Na_2MoS_4> triggered our further interest in assessing the transport properties in these materials, focusing on mixed ionic (ion) and electronic (eon) conducting properties (MIEC, Fig. 5). The direct current-voltage (*d.c.* I-V) measurements are representative of electron conduction, whereas EIS

(electrochemical impedance spectroscopy) provide indication on total conductivity in the sample (SI, MIEC testing and analysis; and Fig. S11). The <Na_2MoS_4> phase has electronic conductivity (σ_{eon}) as high as 6.1 × 10^{-4} S cm^{-1} (at 20°C). EIS analysis confirmed a high degree of electronic conductivity, with equivalent circuits for MIEC failing to provide satisfactory results for the ionic conductivity (σ_{ion}). Considering the low polarization and high rate performances of <Na_2MoS_4> electrodes (see also further discussion) it can be reasonably assumed that this phase is also ion conducting but at lower magnitudes than the electrical conduction given the characteristic EIS response of electronic conductor. Further complex analysis with sophisticated cell and sample configuration including selectively blocking electrodes, for example by use of electron insulating, yet Na-ion conducting contacts, on Na_2MoS_4[40] could provide direct measurements of σ_{ion} in the <Na_2MoS_4> MIEC phase.

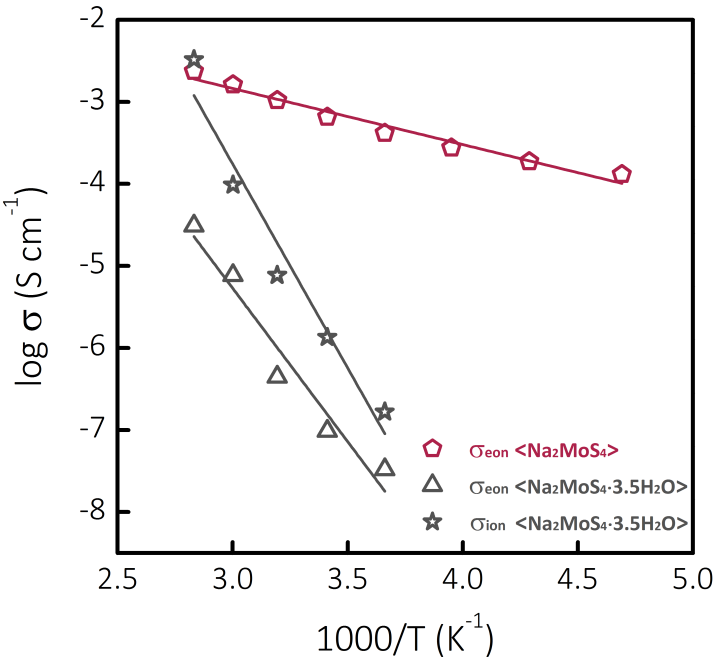

Figure 5. Arrhenius plot of calculated ionic and electronic conductivities in <Na_2MoS_4> and $Na_2MoS_4 \cdot 3.5H_2O$ phases.

The hydrated $Na_2MoS_4 \cdot 3.5H_2O$ phase in turn displayed more pronounced MIEC properties, and EIS analysis combined with *d.c.* measurements allowed separate σ_{ion} and σ_{eon} determination: 1.35 × 10^{-6} S cm^{-1} and 9.27 × 10^{-8} S cm^{-1} at 20°C, respectively. The ionic transport in the hydrated phase is most likely due to Na^+ transfer, as conductivities for proton (H^+) and hydroxide (OH^-) ion are typically orders of magnitude higher. The temperature dependence of the conductivities, follows a linear relationship between the logarithm of the

conductivity with respect to the reciprocal of the temperature in the Arrhenius plot and gives the activation energy (Ea) for each sample: <Na_2MoS_4>_eon = 136 meV; Na_2MoS_4•3.5H_2O_eon = 742 meV and Na_2MoS_4•3.5H_2O_ion = 986 meV. The ionic activation energy for Na_2MoS_4•3.5H_2O is typical of solid electrolytes and proton conductors, being within the same range of our measured values.[41,42] We acknowledge however, that our conductivities are in the lower range for Li^+ / Na^+, more so to proton conductors, and this could be attributed to the amorphous nature of our material. The electronic activation energy for both the hydrated and dehydrated phase are typical of MIEC and are comparable to literature values.[43,44]

With the stable and reversible mixed cationic and anionic redox mechanism in <Na_2MoS_4> confirmed, we continued our analysis on the charge storage performance in lithium half-cells. Since the electronic conductivity of <Na_2MoS_4> was found to be higher than of several conventional inorganic materials (e.g. $Li_4Ti_5O_{12}$ - 10^{-13} S cm^{-1}, $LiFePO_4$ - 10^{-9} S cm^{-1} or $LiMn_2O_4$ - 10^{-6} S cm^{-1})[45] we assembled and cycled <Na_2MoS_4> electrodes with no conductive carbon additives. The electrochemical performance with varying mass fractions of super P carbon (SP) in the composite electrodes at a cycling rate of C/5, and in the extended electrode potential cycling window of 1.4 – 3.0 V vs. Li^+/Li^0 are shown in Figure 6. A charge capacity of ~280 mAh g^{-1} was attained for the pure <Na_2MoS_4> electrodes. As mentioned earlier, the OCP of the assembled cells was around 2.1 V *vs.* Li^+/Li^0 (Fig. 2). The tests in Figures 6A and 6B were started in discharge mode so that only a part of the storage capacity is accessed. During the following charge, the recovered capacity is considerably higher than the one delivered during the preceding step given that the electrode potential window is extended and additional redox is enabled. As expected, the capacity gradually increases up to 460 mAh g^{-1} as the SP content is increased to 30 wt.% explained by better active material utilization, with also lower polarization while increasing the amount of SP. The capacity retention seems to be minimally affected by the amount of the carbon additive, with 74% of the capacity retained for the electrode without SP, comparable to those with SP (85% for 30 wt.% SP) attained after 10 cycles at C/5 rate. At already 10 wt.% conductive agent percolation is attained and no impact on electrode polarization of further increase can be noticed.

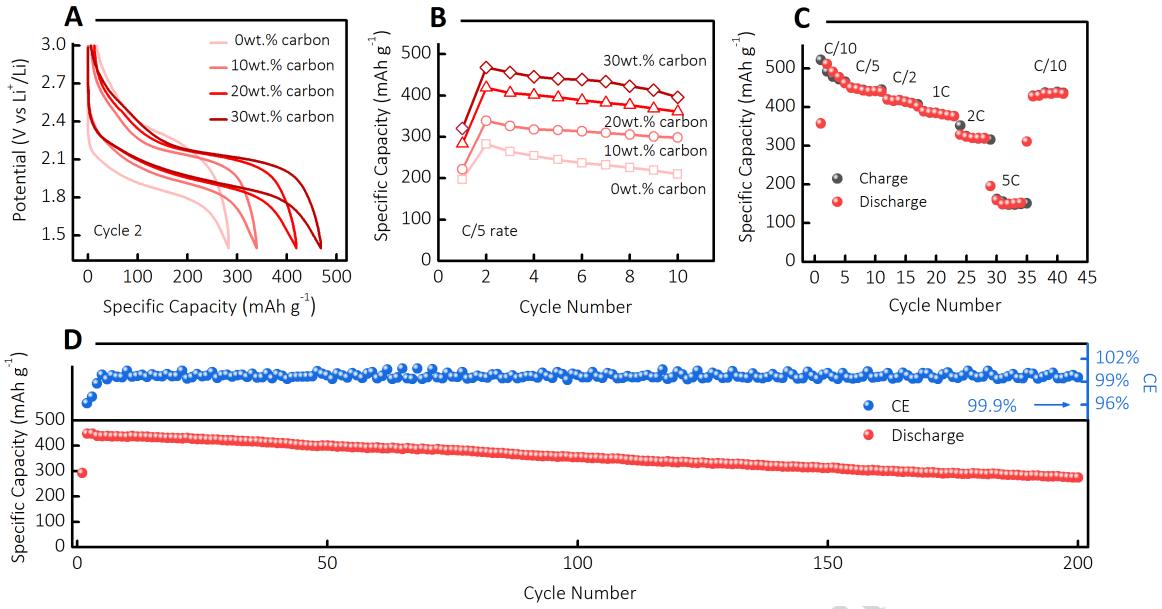

Figure 6. Charge storage performances of <Na_2MoS_4> electrodes. (A) Composition voltage profiles of <Na_2MoS_4> electrodes with different carbon content cycled at a rate of C/5 in the extended cycling window of 1.4-3.0 V vs. Li^+/Li^0 (second cycle is shown). High capacity and acceptable electrode polarization are attained even with no conductive carbon added given the elevated intrinsic electrical conductivity. (B) Corresponding capacity retention plots. Variable-rate performance test (C) and associated extended capacity retention at 1C-rate (D) with cycling for 30 wt.% carbon contained electrodes.

The <Na_2MoS_4> based electrodes also display excellent rate capability (Fig. 6C), achieving 486, 445, 414, 383, 325 and 152 mAh g^{-1}, at cycling rate of C/10, C/5, C/2, 1C, 2C and 5C, respectively. A capacity of 435 mAh g^{-1} is recovered at the end of variable rate test (at C/10) further confirming the excellent rate capability and capacity retention which clearly benefits from the intrinsic electrical conductivity of <Na_2MoS_4>. The long-term cycling performance in Figure 6D shows a high initial capacity of 450 mAh g^{-1} with a capacity retention of 275 mAh g^{-1} over 200 cycles, with also excellent averaged coulombic efficiency of 99.9% maintained along the cycling.

Conclusion

In this work we analyze and demonstrate the feasibility of mixed anionic and cationic reversible redox activity in a Na-rich amorphous coordination polymer of <Na_2MoS_4> composition. Based on cumulative cationic and anionic redox activity, a sustained reversible capacity close to ~ 500 mAh g^{-1} at an average potential of ~ 2.0 V vs. Li^+/Li^0 or of ~ 1.7 V vs.

Na^+/Na^0, is attained. As much as 5 electrons (or corresponding Li or Na cations) can be stored per formula unit, with the redox state of MoS_4^{z-} framework ranging from $z < 1$ to $z > 5$. According to galvanostatic titration and ex-situ XPS analysis, a predominant anionic sulfide redox occurs above 2V (vs. Li^+/Li^0) whereas Mo redox is taking place at lower potentials. We also investigated the transport properties of both <Na_2MoS_4> and $Na_2MoS_4 \bullet 3.5H_2O$, using *d.c.* and *a.c.* methods and found that they are of a mixed ionic electronic conductor type. Our investigation highlights an additional chemistry to explore the importance of sulfur together with the 4d transition metal redox. Although this system shows very high specific capacities, the low redox potential in average may still limit the specific energy for practical application. New approaches can be envisioned, with the use of more abundant 3d metals, yet at the expense of lower capacities, or higher voltage systems on designing double anion systems, for instance based on oxy-sulfides.[46] A complementary route can be the exploration of bimetallic transition metal systems, with for example $Co(MoS_4)_2^{3-}$ or $Fe(MoS_4)_2^{3-}$ complex anions, stabilized by organic tetraethyl ammine cations, being reported.[47] Since the alkali metal cation salts of these have been not reported yet, these make interesting systems to be studied with already an average charge per tetrathiomolybdate anions of -2.5, as well as potentially accessing redox of all three constituent elements - Fe, Mo, and S - for ever-increasing demand of higher energy batteries.

References

[1] B. Dunn, H. Kamath, J. M. Tarascon, *Science* **2011**, *334*, 928–935.

[2] M. Li, J. Lu, Z. Chen, K. Amine, *Adv. Mater.* **2018**, *30*, 1–24.

[3] J. Cabana, L. Monconduit, D. Larcher, M. R. Palacín, *Adv. Mater.* **2010**, *22*, E170–E192.

[4] M. Armand, J.-M. Tarascon, *Nature* **2008**, *451*, 652–657.

[5] R. Schmuch, R. Wagner, G. Hörpel, T. Placke, M. Winter, *Nat. Energy* **2018**, *3*, 267–278.

[6] S. Fang, D. Bresser, S. Passerini, *Adv. Energy Mater.* **2020**, *10*, 1902485.

[7] K. Mizushima, P. C. Jones, P. J. Wiseman, J. B. Goodenough, *Mater. Res. Bull.* **1980**, *15*, 783–789.

[8] G. G. Amatucci, J. M. Tarascon, L. C. Klein, *Solid State Ionics* **1996**, *83*, 167–173.

[9] J. Cho, Y. J. Kim, B. Park, *Chem. Mater.* **2000**, *12*, 3788–3791.

[10] T. Ohzuku, Y. Makimura, *Chem. Lett.* **2001**, *30*, 642–643.

[11] E. McCalla, A. M. Abakumov, M. Saubanère, D. Foix, E. J. Berg, G. Rousse, M. L. Doublet, D. Gonbeau, P. Novák, G. Van Tendeloo, R. Dominko, J. M. Tarascon, *Science* **2015**, *350*, 1516–1521.

[12] M. Sathiya, G. Rousse, K. Ramesha, C. P. Laisa, H. Vezin, M. T. Sougrati, M. L. Doublet, D. Foix, D. Gonbeau, W. Walker, A. S. Prakash, M. Ben Hassine, L. Dupont, J. M. Tarascon, *Nat. Mater.* **2013**, *12*, 827–835.

[13] C. S. Johnson, N. Li, C. Lefief, J. T. Vaughey, M. M. Thackeray, *Chem. Mater.* **2008**, *20*, 6095–6106.

[14] K. Luo, M. R. Roberts, R. Hao, N. Guerrini, D. M. Pickup, Y. S. Liu, K. Edström, J. Guo, A. V. Chadwick, L. C. Duda, P. G. Bruce, *Nat. Chem.* **2016**, *8*, 684–691.

[15] Z. Shadike, Y. N. Zhou, L. L. Chen, Q. Wu, J. L. Yue, N. Zhang, X. Q. Yang, L. Gu, X. S. Liu, S. Q. Shi, Z. W. Fu, *Nat. Commun.* **2017**, *8*, 1–9.

[16] T. Wang, G.-X. Ren, Z. Shadike, J.-L. Yue, M.-H. Cao, J.-N. Zhang, M.-W. Chen, X.-Q. Yang, S.-M. Bak, P. Northrup, P. Liu, X.-S. Liu, Z.-W. Fu, *Nat. Commun.* **2019**, *10*, 4458.

[17] S. Saha, G. Assat, M. T. Sougrati, D. Foix, H. Li, J. Vergnet, S. Turi, Y. Ha, W. Yang, J. Cabana, G. Rousse, A. M. Abakumov, J. M. Tarascon, *Nat. Energy* **2019**, *4*, 977–987.

[18] C. J. Hansen, J. J. Zak, A. J. Martinolich, J. S. Ko, N. H. Bashian, F. Kaboudvand, A. Van der Ven, B. C. Melot, J. Nelson Weker, K. A. See, *J. Am. Chem. Soc.* **2020**, *142*, 6737–6749.

[19] Z. Li, B. P. Vinayan, P. Jankowski, C. Njel, A. Roy, T. Vegge, J. Maibach, J. M. G. Lastra, M. Fichtner, Z. Zhao-Karger, *Angew. Chem. Int. Ed.* **2020**, *59*, 2–10.

[20] J. Rouxel, *Chem. - A Eur. J.* **1996**, *35*, 1053–1059.

[21] J. Wu, D. Wang, H. Liu, W.-M. Lau, L.-M. Liu, *RSC Adv.* **2015**, *5*, 21455–21463.

[22] S. S. Zhang, D. T. Tran, *J. Mater. Chem. A* **2016**, *4*, 4371–4374.

[23] S. Britto, M. Leskes, X. Hua, C. A. Hébert, H. S. Shin, S. Clarke, O. Borkiewicz, K. W. Chapman, R. Seshadri, J. Cho, C. P. Grey, *J. Am. Chem. Soc.* **2015**, *137*, 8499–8508.

[24] J. B. Goodenough, Y. Kim, *J. Solid State Chem.* **2009**, *182*, 2904–2911.

[25] J. Xu, J. Zhang, W. Zhang, C.-S. Lee, *Adv. Energy Mater.* **2017**, *7*, 1700571.

[26] G. F. Khudorozhko, L. G. Bulusheva, L. N. Mazalov, V. E. Fedorov, J. Morales, E. A. Kravtsova, I. P. Asanov, G. K. Parygina, Y. V. Mironov, *J. Phys. Chem. Solids* **1998**, *59*, 283–288.

[27] K. M. Abraham, *J. Electrochem. Soc.* **1987**, *134*, 2661.

[28] D. Pasquariello, K. . Abraham, *Mater. Res. Bull.* **1987**, *22*, 37–44.

[29] D. Bélanger, G. Laperriére, B. Marsan, *J. Electroanal. Chem.* **1993**, *347*, 165–183.

[30] R. N. Bhattacharya, C. Y. Lee, F. H. Pollak, D. M. Schleich, *J. Non. Cryst. Solids* **1987**, *91*, 235–242.

[31] S. H. Laurie, D. E. Pratt, J. H. L. Yong, *Inorganica Chim. Acta* **1984**, *93*, 57–59.

[32] D. Genuit, P. Afanasiev, M. Vrinat, *J. Catal.* **2005**, *235*, 302–317.

[33] D. Aurbach, I. Weissman, A. Zaban, P. Dan, *Electrochim. Acta* **1999**, *45*, 1135–1140.

[34] T. Kawamura, S. Okada, J. Yamaki, *J. Power Sources* **2006**, *156*, 547–554.

[35] Q. D. Truong, L.-C. Yin, N. T. Hung, D. N. Nguyen, Y. Gambe, K. Nayuki, Y. Sasaki, H. Kobayashi, R. Saito, P. D. Tran, I. Honma, *Electrochim. Acta* **2020**, *332*, 135218.

[36] N. T. Hung, L.-C. Yin, P. D. Tran, R. Saito, *J. Phys. Chem. C* **2019**, *123*, 30856–30862.

[37] J. Baltrusaitis, B. Mendoza-Sanchez, V. Fernandez, R. Veenstra, N. Dukstiene, A. Roberts, N. Fairley, *Appl. Surf. Sci.* **2015**, *326*, 151–161.

[38] C.-H. Lin, C.-H. Tsai, F.-G. Tseng, Y.-Y. Yu, H.-C. Wu, C.-K. Hsieh, *Nanoscale Res. Lett.* **2015**, *10*, 446.

[39] L. Benoist, D. Gonbeau, G. Pfister-Guillouzo, E. Schmidt, G. Meunier, A. Levasseur, *Thin Solid Films* **1995**, *258*, 110–114.

[40] J.-S. Lee, J. Jamnik, J. Maier, *Monatshefte für Chemie - Chem. Mon.* **2009**, *140*, 1113–1119.

[41] P. Colomban, *Solid State Ionics* **2019**, *334*, 125–144.

[42] S. Yubuchi, H. Tsukasaki, A. Sakuda, S. Mori, A. Hayashi, M. Tatsumisago, *RSC Adv.* **2019**, *9*, 14465–14471.

[43] W.-C. Wei, D.-R. Huang, D. Wang, *Materials* **2016**, *9*, 922.

[44] J. Ryu, R. O'Hayre, H. Lee, *J. Mater. Res.* **2014**, *29*, 2667–2672.

[45] Y. Lu, J. Chen, *Nat. Rev. Chem.* **2020**, *4*, 127–142.

[46] V. Yufit, M. Nathan, D. Golodnitsky, E. Peled, *J. Power Sources* **2003**, *122*, 169–173.

[47] W.-H. Pan, D. C. Johnston, S. T. McKenna, R. R. Chianelli, T. R. Halbert, L. L. Hutchings, E. I. Stiefel, *Inorganica Chim. Acta* **1985**, *97*, L17–L19.

Acknowledgments.

Q. Z, J. W. and X. L. acknowledge China Scholarship Council for financial support. This work was also funded by CF-ARC (18/23-093) MICROBAT and F.R.S. FNRS U.N011.18 - DEMIST grant. R.D. acknowledges financial support from European Research Council (ERC, grant agreement no. 770870) for his fellowship. N.E. acknowledges financial support from INNOVIRIS 2019-RDIR-59B for his fellowship. The authors thank Yang FU for assistance with XPS measurements.

Table of Contents

A mixed ion-electron conducting amorphous phase of tetrathiamolybdate - MoS_4^{2-}, with mixed Mo and S valences, shows a sustainable reversible capacity of 500 mAh/g based on cumulative anionic Sulfide and cationic Molybdenum redox. The amorphous nature renders this chemistry equally suitable for Li and Na-cation storage with further avenues to be explored to multivalent as well as higher voltage redox.

Keywords: *Metal ion battery; Amorphous; Metal polysulfides; Sulfur redox; Mixed ionic-electronic conductor; Oxidation; Materials; Electrodes*

Authors : Qi Zhu, Jiande Wang, Xuelian Liu, Dr. Neil Ebejer, Dr. Darsi Rambabu, and Prof. Alexandru Vlad*

Title : Mixed Anionic and Cationic Redox Chemistry in a Tetrathiomolybdate Amorphous Coordination Framework

TOC Graphic :